POLITECNICO DI TORINO
Repository ISTITUZIONALE

Constraining impedance-based controllers: generalised framework and experimental validation

Original
Constraining impedance-based controllers: generalised framework and experimental validation / Paduano, B., Glorioso, M., Dutto, L., Barbera, R., Faedo, N., Mattiazzo, G., Ferri, F.. - In: NONLINEAR DYNAMICS. - ISSN 0924-090X. - 113:14(2025), pp. 18303-18318. [10.1007/s11071-025-11121-3]

Availability:
This version is available at: 11583/2999002 since: 2025-04-10T07:45:46Z

Publisher:
Springer Science and Business Media

Published
DOI:10.1007/s11071-025-11121-3

Terms of use:

This article is made available under terms and conditions as specified in the corresponding bibliographic description in the repository

Publisher copyright

(Article begins on next page)

25 November 2026

Nonlinear Dyn (2025) 113:18303–18318
https://doi.org/10.1007/s11071-025-11121-3

RESEARCH

Constraining impedance-based controllers: generalised framework and experimental validation

Bruno Paduano · Mattia Glorioso · Lorenzo Dutto · Riccardo Barbera · Nicolás Faedo · Giuliana Mattiazzo · Francesco Ferri

Received: 25 November 2024 / Accepted: 11 March 2025 / Published online: 1 April 2025
© The Author(s) 2025

Abstract Wave energy converters (WECs) hold significant potential in the global energy market, though their high energy costs compared to traditional sources remain a challenge. Recent research has focused on power maximisation strategies to make WECs more competitive, with optimisation-based control methods offering one solution. However, these methods are often complex and difficult to implement in real-time scenarios. Simpler, non-optimisation-based approaches, such as impedance based control, have gained interest due to their ease of implementation and ability to provide representative control actions. Despite their advantages, impedance based controllers often suffer from unconstrained control forces, potentially leading to suboptimal performance and exceeding the validity range of the system model. This study introduces a novel constrained impedance based control strategy that maintains the simplicity of traditional methods while addressing the limitations of unconstrained controllers. The proposed approach is experimentally validated using the Wavestar prototype at the Aalborg facility in Denmark, under both monochromatic and panchromatic wave conditions. Results show that the constrained controller effectively confines the device motion within predefined limits, improving power output under nonlinear force saturation. These findings demonstrate that constrained impedance-based control can provide more accurate and practical control actions, enhancing the performance of WECs in real-world applications.

Keywords Wave energy · Control · Experimental testing

B. Paduano (✉)· M. Glorioso · L. Dutto · R. Barbera · N. Faedo · G. Mattiazzo · F. Ferri
Politecnico di Torino, Turin, Italy
e-mail: bruno.paduano@polito.it

1 Introduction

Wave energy converters (WECs) represent a promising technology within the global energy landscape [1,2]. Although the cost of energy from these novel technologies remains high compared to traditional sources, research is advancing towards power maximisation strategies aimed at making WECs competitive in the global energy market. The optimal control problem for WECs can be generally tackled using optimisation-based strategies [3,4], yet these methodologies can be inherently complex (in a computational sense) and can be challenging to implement, particularly for real-time applications[1].

As such, recent years researchers have expressed an increasing interest in non-optimisation-based approaches, which are inherently simpler to implement. These methods allow for representative control actions and performance evaluations through the use and synthesis of so-called *impedance-based* controllers [8,9].

[1] For an extensive description of the control strategies adopted in the wave energy field, the interested reader is referred to [4–7].

Such approaches are attractive due to their simplicity of synthesis. Overall, impedance matching (IM)-based controllers aim to replicate well-known conditions for optimal energy absoprtion under linearity assumptions. In particular, if controlled accordingly, the instantaneous phase of the wave excitation force (i.e. the force exerted by the incoming wave field on the device wetted surface) should be in phase with the device velocity in the controlled degree-of-freedom. While these conditions form the foundation of IM-based controllers, the non-causal nature of such controllers means that the associated energy-maximising strategy can not be implemented directly [10]. To address this issue, the optimal controller structure is typically approximated by leveraging a *stable, causal* structure [11]. Due to their simplicity, impedance-based controllers have been extensively applied in the wave energy field. For instance, in [9], the IM principle is applied and generalised to multi-degree-of-freedom (multi-DoF) systems. In many cases, IM controllers are widely used in experimental campaigns, as they can be synthesised using models derived from experimental data. For example, in [12,13], the controller has been rigorously tested with the Wavestar devices during the so-called wave energy control competition. In [14], an IM-based controller is designed during an experimental campaign in-situ, to achieve a representative control action, utilising a data-based modelling approach to synthesise the controller while accounting for prototyping uncertainties [15]. In this case, the controlled device is a multi-DoF system, where the two controlled DoFs are not the hydrodynamic ones. Consequently, [14] provides a representative experimental application of the IM principle. Another experimental application of IM-based controllers is presented in [16], where such controllers are utilised to control both heaving and flap devices. This control synthesis procedure, with its inherent simplicity, is also employed in [17], where a moored point absorber is optimised in a co-design fashion, achieving a significant computational advantage through IM theory.

However, these controllers not only rely on linearity, but any physical limitations are fully ignored within the design and synthesis procedure, and the controller is derived in unconstrained conditions. For example, in [18], an impedance-matching controller is compared to a pseudo-spectral technique under monochromatic conditions, highlighting the inability of the former to limit the device response. The unconstrained nature of such control strategies may prove limiting, as they can result in the controller pushing the system outside the identified model validity range, leading to a non-representative control action, a situation referred to as the modelling paradox [19,20]. Moreover, if force saturations are present, as is typical in real-world control actions, the effectiveness of the synthesised control force may be diminished, resulting in performance overestimation. This problem is well-recognised in the literature, with a common solution being resourcing to an iteratively tuning of the controller parameters. For instance, in [21], a two-device array is tested using a controller synthesised as the system complex-conjugate impedance. The resulting controller is tuned in regular wave conditions to limit device excursion, yet this approach ultimately compromises the impedance-matching conditions, i.e. the velocity is no longer in phase with the excitation force. The impedance-matching principle can also be applied to synthesise a feedforward controller for panchromatic excitation conditions, as demonstrated with the LiTe-Con approach [22]. However, the constraint methodologies developed thus far primarily rely on suboptimal constraint-handling mechanisms, which are implemented after the controller synthesis [23].

It is also important to mention anti-windup constraint approaches. These methods [24] are designed to mitigate the windup effect caused by saturations and hard-stops, which can lead to a loss of system stability and a decrease in the representativeness of the modelled system. In such cases, constraints are applied by leveraging a state prediction through a tailored limitation logic. An application of this approach to wave energy systems is detailed in [25]. Nonetheless, the constraint handling methodologies available are often ad-hoc, and the result of constraining the solution a-posteriori, as opposed to incorporating information on the device limitations within the synthesis procedure itself. This, naturally, can drastically change the expected energy outcome, significantly shifting from the idealised impedance-matching operational conditions.

Motivated by this, we present, within this paper, a systematic approach to incorporate constraint information (and handling) within impedance-matching-based control synthesis for WECs, offering the following contribution:

– A soft constraint handling approach is proposed, inherently embedded within impedance-matching theory. The goal is to maintain simplicity within the control synthesis procedure, while still respecting the impedance phase condition. The mathematical formulation is presented alongside a description of the synthesised controller for both monochromatic and panchromatic excitation conditions. Then, the developed mathematical formulation is applied and analysed experimentally during an experimental investigation conducted in Aalborg University, Denmark. The Wavestar device is tested by evaluating its response under both constrained and unconstrained conditions, providing a detailed assessment of the controller's performance and its ability to manage the device's motion effectively.

Before delving into the analysis, we wish to emphasise the potential of this control strategy for quantifying system performance during experimental investigations [14,21]. The development of operational environments necessitates wave tank tests [26], which are crucial for understanding system responses under real-world conditions. Although numerical wave tanks [27,28] present a promising approach for defining representative system responses, they remain constrained by the high computational burden required. Particularly when aiming to quantify system power absorption under sufficiently long panchromatic wave conditions, experimental testing in wave tanks is indispensable. However, the presence of constraints can prove significantly limiting, especially when defining the overall system performance. Finally, for the sake of clarity, we would like to remark that while this study employs a linear controller, more advanced modelling techniques capable of handling nonlinear constraints are also considered in the wave energy field. The interested reader is referred to [4–7].

The remainder of this manuscript is organised as follows: Sect. 2 provides a general description of the application of the IM principle to multi-input-multi-output (MIMO) systems (Sect. 2.1), with an analysis of the matching frequency in Sect. 2.2. The constraint approach is presented in Sect. 2.3. Section 3 details the experimental campaign, including the layout (Sect. 3.1), the test schedule and objectives (Sect. 3.2), and performance results (Sect. 3.3). Finally, the conclusions are summarised in Sect. 4.

1.1 Notation

With $\mathbb{R}^+$, the set of positive real numbers is represented. With $\mathbb{N}^+$, the set of non-zero natural number is defined, i.e. $\mathbb{N}^+ = \{1, 2, \ldots, \infty\} \subset \mathbb{N}$. $\mathbb{I}$ denotes the identity matrix of conformable dimensions, according to the context. $F(\omega) = \mathcal{F}(f(t))$ represents the Fourier transform of the function f. Moreover, whenever a function is represented by a Greek letter, its Fourier transform is indicated with *tilde*, e.g. the Fourier transform of the η is expressed with $\tilde{\eta}$. Given a matrix $A \in \mathbb{C}^{n\times m}$, $A^* \in \mathbb{C}^{m\times n}$ represents the conjugate transpose of A. Additionally, given a square non-singular matrix $B \in \mathbb{C}^{n\times n}$, $(B^*)^{-1} \in \mathbb{C}^{n\times n}$ denotes the inverse Hermitian of B. With the notation $A^\dagger \in \mathbb{C}^{m\times n}$ the Moore-Penrose pseudo-inverse of a matrix A is denoted. Given a matrix $A \in \mathbb{C}^{n\times m}$, and a matrix $B \in \mathbb{C}^{n\times m}$, $A \circ B$ denotes the Hadamard product of the matrices.

2 A generalised constrained approach for impedance-based controllers

In this section, the proposed methodology is discussed and presented. To keep this manuscript reasonably self-contained, we begin by providing a generic description of the IM principle and its application in the wave energy field. We would like to begin by emphasising the IM principle, which forms the foundation of this study. Originating from electrical engineering [8], the principle asserts that to maximise energy transfer, a given electric load should be designed to match the complex conjugate of the system impedance. Given the inherently simplicity, this theory is widely applied in wave energy field [9,16,22]. However, since the developed theory is effectively model-based, before delving into the specifics of this section, we provide a brief modelling-oriented description of wave energy systems, useful for the definition of the corresponding impedance.

A generic wave energy system can be described using a schematic representation, as depicted in Fig. 1 (a). In this figure, $\eta : \mathbb{R} \to \mathbb{R}, t \mapsto \eta(t)$ represents the wave elevation, and $f_e : \mathbb{R} \to \mathbb{R}^n, t \mapsto, f_e(t)$, $f_{\text{ext}} : \mathbb{R} \to \mathbb{R}^n, t \mapsto f_{\text{ext}}(t), \dot{x} : \mathbb{R} \to \mathbb{R}^n, t \mapsto \dot{x}(t)$ denote the wave excitation force, a generic external action, and the system velocity, respectively, where n is the number of degrees of freedom (DoFs) of the system. This description of the forces involved allows the

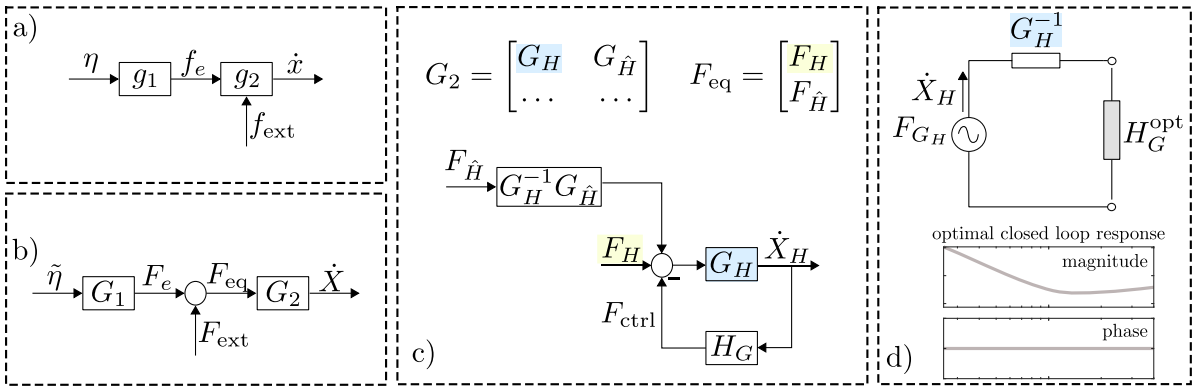


Fig. 1 Synthesis of the impedance-based controller: a) Schematic description of the real WEC; b) Linearised description of the WEC; c) MIMO system description outlining the direct link (in blue), and the force acting directly on the controlled DoFs (in yellow); equivalent electrical circuit representation and optimal closed-loop response

wave energy system to be decoupled, into two mappings, $g_1 : \eta \mapsto f_e$ and $g_2 : f_e, f_{\text{ext}} \mapsto \dot{x}$, defining the relationship between wave elevation and excitation force, and between force and velocity, respectively. This wave energy system representation is ubiquitous in the marine field, as it is associated with a low-fidelity model and its corresponding linear representation (denoted by G_1 and G_2), and relies on so-called linear potential flow theory [29,30].

2.1 Impedance-based controller for MIMO systems

From a general perspective, the controller for an underactuated multi-DoF device can be synthesised as described in [9].

This formulation is schematically depicted in Fig. 1, and can be summarised as follows:

1. A generic wave energy system is pursued. To maintain generality, the system is represented as broadly as possible, in terms of the linear maps G_1 and G_2.
2. For a generic underactuated system $\{n, n_c\} \subset \mathbb{R}^+$ represent the overall system and controlled DoFs, respectively, with $n_c \leq n$. The system map $G_2 \in \mathbb{C}^{n \times n}$ is organised, without any loss of generality, to expose the controlled DoFs in terms of the first rows. The direct link $G_H \in \mathbb{C}^{n_c \times n_c}$ is highlighted, upon which an equivalent force F_{G_H} acts, defined as:
$$F_{G_H} = F_H + G_H^{-1} G_{\hat{H}} F_{\hat{H}}, \tag{1}$$
where $F_H \in \mathbb{C}^{n_c}$ is the force acting on the controlled DoFs, $F_{\hat{H}} \in \mathbb{C}^{n-n_c}$ is the force acting on the uncontrolled DoFs, and $G_{\hat{H}} \in \mathbb{C}^{n_c \times (n-n_c)}$ represents the coupling term between the controlled and uncontrolled DoFs.
3. Finally, leveraging the electrical analogy, the optimal controller can be synthesised as the complex conjugate of the system impedance:
$$H_G = H_G^{\text{opt}} = (G_H^*)^{-1}, \tag{2}$$
where G_H^{-1} is the system impedance. Please note that given the physical nature of the mapping G_H, the associated frequency-response is virtually always characterised in terms of a symmetric operator [31]. We would like to remark that the optimal closed-loop works as an ideal zero-phase filter, in which the velocity is *in-phase* with the exciting force, and can be expressed as:
$$T^{opt} = G_H G_H^* (G_H + G_H^*)^{-1}, \tag{3}$$
with the output velocity representing a frequency-dependant scaled version of the force F_{G_H}.

Remark 1 It is important to note that, for the derivation of the IM principle, the mapping G_2 needs to be I/O stable, strictly proper, minimum-phase, and positive-real. Although this assumption ensures that the derived controller is stable, it is inherently *anti-causal*, as it requires knowledge of future input conditions to achieve optimal energy absorption. This issue is typically addressed by interpolating the optimal controller response, for a given matching frequency, with a stable controller structure [9,32], i.e. matching a given controller structure *locally* to the optimal anti-causal one.

To conclude, although controller stability can be guaranteed by the properties of the map G_H, the stability of the closed-loop system requires a separate consideration. Furthermore, since the controller interpolating structure is not necessarily defined *a priori*, additional considerations must be addressed on a case-by-case basis. As wave energy systems are inherently passive (i.e., the map G_H is passive), one possibility is enforce passivity in the controller synthesis procedure, to ensure closed-loop stability [33].

2.2 On the matching frequency in panchromatic conditions

While the definition of the matching frequency, i.e. the point in which the ideal anti-causal controller response is matched with an implementable causal structure (see Remark 1), can be straightforward when the system is excited by monochromatic conditions (regular waves for wave energy systems), it becomes more challenging under panchromatic conditions. Therefore, to circumnavigate this issue, in most applications, the matching frequency is often identified as the peak (or another characteristic frequency) of the wave spectrum [14,32,34]. However, as described in [35,36], the controller should be designed by analysing the input condition F_{G_H}. In other words, the matching frequency should correspond to a characteristic frequency of the force spectrum, which does not necessarily correspond with that characterising the wave spectrum itself.

While in many cases, the definition of the input exciting spectra can be easily obtained by leveraging, for example, excitation force coefficients [35] derived from boundary element software [29], the process can become more complex due to the mutual interactions among DoFs. This complexity is particularly heightened when the controlled DoF does not correspond to a hydrodynamic mode, i.e., the DoFs that directly respond to wave forces. Non-hydrodynamic DoFs, which are not directly influenced by wave interactions, present extensive challenges due to the distinct nature of their coupling among modes [36].

Following the procedure described in [36], the linear model can be represented as a wave-to-force and a force-to-motion map, focusing solely on the controlled DoFs. This analysis can also be conducted experimentally, as the G_H map can be obtained by *exciting* the controlled DoFs [9], and the wave-to-force map can be derived using the so-called free motion (i.e. uncontrolled) tests, as follows:

$$G_{\hat{1}} = G_H^{-1} G_\star, \tag{4}$$

where $G_{\hat{1}} \in \mathbb{C}^{n_c}$ is the wave-to-force map, and $G_\star \in \mathbb{C}^{n_c}$ represents the link between wave elevation and the system response. Consequently, the spectra of the exciting condition can be obtained from the wave spectra, as follows:

$$S_{F,i} = G_{\hat{1},i} G^*_{\hat{1},i} S_\eta, \tag{5}$$

where $S_{F,i} : \mathbb{R}^+ \to \mathbb{R}, \omega \mapsto S_{F,i}(\omega)$ represents the spectrum of the exciting action $F_{G_H,i}$, and $S_\eta : \mathbb{R}^+ \to \mathbb{R}, \omega \mapsto S_\eta(\omega)$ represents the wave spectrum, with $i \in [1, \ldots, n_c]$. Although the exciting spectra can be easily defined in terms of (5), identifying a matching frequency is not straightforward. If the controlled DoFs are characterised by significantly different exciting conditions, the matching frequency should be determined as part of the energy-maximisation procedure itself. However, this represents a peculiar case that is difficult to characterise in practice. Typically, even when multiple DoFs are involved, these tend to 'resemble' each other (i.e. they are dynamically similar, such in [34]), resulting in a simpler definition of the matching frequency.

2.3 A constraint handling approach

So far, the IM methodology defines a straightforward approach to synthesising an effective controller while avoiding complex numerical routines. Nevertheless, the control actions are designed to maximise the harvested energy without considering any possible technological limits, i.e. the IM matching conditions are fully derived without considering constraints.

In a real wave energy system, technological constraints can limit the system position, velocity, and/or force applied by the power take-off (PTO, i.e. generator). In order to include this information as part of the IM synthesis procedure, within this study, a constraint-handling methodology is proposed, that aims to limit the standard deviations of key variables:

$$\Omega : \begin{cases} \sigma_{x_{H,i}} & < \sigma_{x_{H,des,i}}, \\ \sigma_{\dot{x}_{H,i}} & < \sigma_{\dot{x}_{H,des,i}}, \\ \sigma_{f_{ctrl,i}} & < \sigma_{f_{ctrl,des,i}}, \end{cases} \tag{6}$$

where $i \in [1, \ldots, n_c]$ represents the controlled DoFs, $\{x_{H,i}, \dot{x}_{H,i}, f_{ctrl,i}\} \subset \mathbb{R}^+$ are the position, velocity,

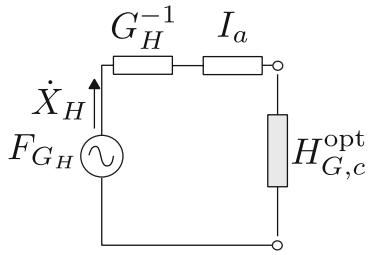


Fig. 2 Impedance-matching electric scheme modified by adding a properly tuned impedance

and control force associated to the controlled DoF i^{th} and, finally, σ represents the associated standard deviation. A feasible solution to the constrained control problem can be achieved through various approaches. Although more complex strategies can be employed for constrained control synthesis (e.g., model predictive control), in this study, the controller is synthesised by adding a properly tuned impedance to the system, in an effort to keep the simplicity of non-optimisation-based controllers for WECs.

In particular, by leveraging the impedance-matching theory, the force-to-velocity closed-loop map acts as an ideal zero-phase filter (see Sect. 2.1), so the added impedance needs to be modulated to maintain the phase condition. Thus, the magnitude of the resulting controller map is a scaled version of the optimal one.

In Fig. 2, the electrical analogy is shown, where G_H^{-1} is the system impedance, and $\{H_{G,c}^{\text{opt}}, I_a\} \subset \mathbb{C}^{n_c \times n_c}$ represent the optimal constrained controller, i.e. $H_{G,C}^{\text{opt}} = (G_H^*)^{-1} + I_a^*$, and the added impedance. To preserve the phase condition in the force-to-velocity closed-loop system, the added impedance needs to be tailored to the closed-loop, i.e.,

$$\begin{aligned} T_c^{\text{opt}} &= (G_H H_{G,C}^{\text{opt}} + \mathbb{I})^{-1} G_H \\ &= \left((G_H^*)^{-1} + I_a^* + G_H^{-1}\right)^{-1}. \end{aligned} \tag{7}$$

In most applications, the map G_H is symmetric (due to the axisymmetric behaviour of the dynamic interactions between different modes of motion, see [9,31]), and therefore, by leveraging this assumption (i.e., $G_H = G_H^*$), it is possible to appreciate that the map T_c^{opt} behaves as an ideal filter if the added impedance I_a is symmetric and has no imaginary part, i.e., $I_a = I_a^* \in \mathbb{R}^{n_c \times n_c}$.

Taking into account (7), the added impedance must be tuned with respect to the system constraints. Accordingly, the equation linking the input force to the velocity is:

$$\begin{aligned} \dot{X}_H &= \left(G_H H_{G,C}^{\text{opt}} + \mathbb{I}\right)^{-1} G_H F_{G_H} \\ &= \left(G_H \left((G_H^*)^{-1} + I_a^*\right) + \mathbb{I}\right)^{-1} G_H F_{G_H}, \end{aligned} \tag{8}$$

which leads to

$$(G_H \left((G_H^*)^{-1} + I_a^*\right) + \mathbb{I}) \dot{X}_H = G_H F_{G_H}, \tag{9}$$

and, finally,

$$I_a \approx F_{G_H,0} \dot{X}_{H,0}^{\dagger} - (G_H^{-1} + (G_H^*)^{-1}), \tag{10}$$

where $\dot{X}_{H,0}^{\dagger}$ represents the Moore-Penrose pseudo-inverse of $\dot{X}_{H,0}$. By leveraging the zero-phase condition that links the exciting input F_{G_H} with the system output $\dot{X}_H$, it is possible to evaluate the added impedance used in the control synthesis to verify a given output amplitude condition $\dot{X}_{H,0}$. Which means that, in monochromatic exciting condition the problem Ω leads to the definition of $X_{H,i} = X_{H,des,i}$. Please note that the definition of the system response under monochromatic exciting conditions is consistently considered in the wave energy field for analysing performance and identification purposes [37,38]. The choice of exciting wave energy devices (numerically and experimentally) with a monochromatic signal is made to investigate the system response while mitigating nonlinear effects caused by distortions, such as second-order wave phenomena [30].

However, while the amplitude definition can be achieved as described above, ocean waves are characterised by a broad frequency range, so they are generally defined statistically by means of a spectrum.[2] The system response can be analysed by leveraging the wave input spectrum, i.e.,

$$S_{\dot{X}_{H,i}} = G_{\star,i} G_{\star,i}^* S_\eta, \tag{11}$$

where $S_{\dot{X}_{H,i}} : \mathbb{R} \to \mathbb{R}, \omega \mapsto S_{\dot{X}_{H,i}}(\omega)$ represents the velocity spectrum. Accordingly, the position and control force spectra can be defined as:

$$\begin{aligned} S_{X_{H,i}} &= \left(\frac{1}{j\omega} G_{\star,i}\right) \left(\frac{1}{j\omega} G_{\star,i}\right)^* S_\eta, \\ S_{F_{G_H,i}} &= (G_\star H_G)_i (G_\star H_G)_i^* S_\eta, \end{aligned} \tag{12}$$

[2] It is important to note that the excitation input force F_{G_H} does not represent the wave excitation force but rather the forces acting on the actuated axes.

which can be used to express the constraints defined in Ω as:

$$\Omega : \begin{cases} \int_{\mathbb{R}^+} S_{\dot{X}_{H,i}}\, d\omega \leq \sigma^2_{\dot{X}_{H,des,i}}, \\ \int_{\mathbb{R}^+} S_{X_{H,i}}\, d\omega \leq \sigma^2_{X_{H,des,i}}, \\ \int_{\mathbb{R}^+} S_{F_{G_H},i}\, d\omega \leq \sigma^2_{F_{G_H},des,i}, \end{cases} \tag{13}$$

where $\int_{\mathbb{R}^+} S_{\dot{X}_H,i}\, d\omega = \sigma^2_{\dot{X}_{H,i}}, i \in [1, \ldots, n_c]$ represents the squared variance of the associated signal. Using the equations in (13), it is not possible to directly determine the added impedance matrix I_a, as this would require n_c^2 equations. However, the problem can be bypassed by defining the added impedance as a function of the real part of the system impedance, i.e., $\Re(G_H^{-1})$. This yields:

$$\begin{aligned} T_c^{\text{opt}} &= \left(G_H^{-1} + (G_H^*)^{-1} + I_a\right)^{-1}, \\ I_a &= V_\alpha \circ \Re(G_H^{-1}), \\ v_\alpha &= \left[\alpha_1 \ \ldots \ \alpha_{n_c}\right]^\intercal. \end{aligned} \tag{14}$$

Being, $v_\alpha \in \mathbb{R}^{n_c}$ and $V_\alpha = v_\alpha \otimes \mathbf{1}_{n_c}$ where $\mathbf{1}_{n_c}$ is a row vector of ones of dimension $1 \times n_c$, and $\otimes$ denotes the outer product, resulting in an $n_c \times n_c$ matrix. Each column of V_α is a replication of v_α, enabling element-wise multiplication with $\Re(G_H^{-1})$. Furthermore, $\alpha_i \in \mathbb{A} \subset \mathbb{R}$ defines an equation that satisfies the constraints of a DoF (see Eq. 13), with $\mathbb{A} = (-1, +\infty)$. Please note that, given that G_H matrix has non-zero off-diagonal elements, the coupling between controlled DoFs cannot be neglected, and the associated response must be considered using the system singular values. Please note that, while the classic synthesis of an unconstrained IM-based controller is instantaneous, requiring only the computation of the complex conjugate operator of the system impedance, the proposed methodology involves an iterative process (see Equation (13)). However, despite the iterative nature of the calculation, the computational burden remains quite manageable. For instance, the computational time required to define the added impedance in this study ranged from 0.1 to 0.2 s on a laptop equipped with an Intel i7 CPU. Although the influence in a multi-DoF system can be observed by investigating the sigma plot of a controlled DoF, Fig. 3 illustrates the influence of the added impedance on a SISO system. Note that, to maintain constraints on the system velocity, the magnitude of the controller map increases as resistance increases, and the associated closed-loop map magnitude decreases accordingly. The reduction in the magnitude of the closed-loop frequency response results in a diminished system response (i.e., motion), thereby creating a constrained condition.

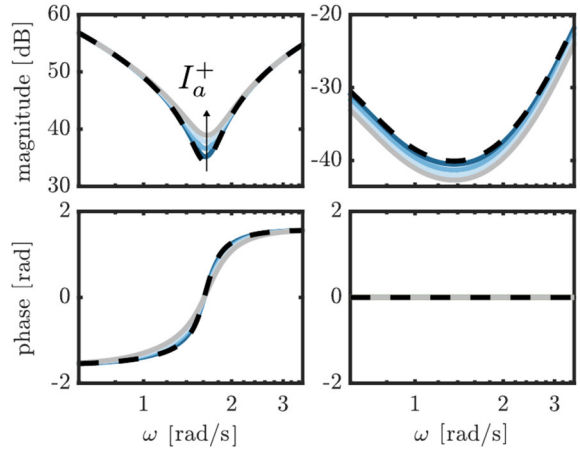


Fig. 3 System response under the influence of added impedance I_a, according to a generic system as described in Fig. 1. On the left-hand side, the controller map H_G is shown, and on the right-hand side, the closed-loop response

3 Experimental investigation

Following the development of the constraint handling condition within IM-based controller synthesis for WECs, within this section, a detailed description of the experimental campaign and the associated tests, used for assessment and validation of the proposed technique, is provided. In Sect. 3.1, the wave facility is discussed, with an analysis of the wave tank properties and the adopted prototype. Section 3.2 outlines the experimental tests, including their objectives and methodologies. Finally, the results obtained from the controlled device are highlighted in Sect. 3.3.

3.1 Tank facility and prototype description

In this experimental campaign, the wave tank facilities utilised to achieve the desired objectives and to effectively test the presented control approach are located at the Ocean and Coastal Engineering Laboratory, Aalborg University, Denmark. Specifically, the facilities feature a basin with dimensions of 19.3 [m] × 14.6 [m] × 1.5 [m] (length × width × depth), with an active testing area of 13 [m] × 8 [m] (length × width). The WEC system selected for this experimental campaign is a 1:20 scale model of the Wavestar wave energy conversion system [39]. The prototype, shown in Fig. 4,

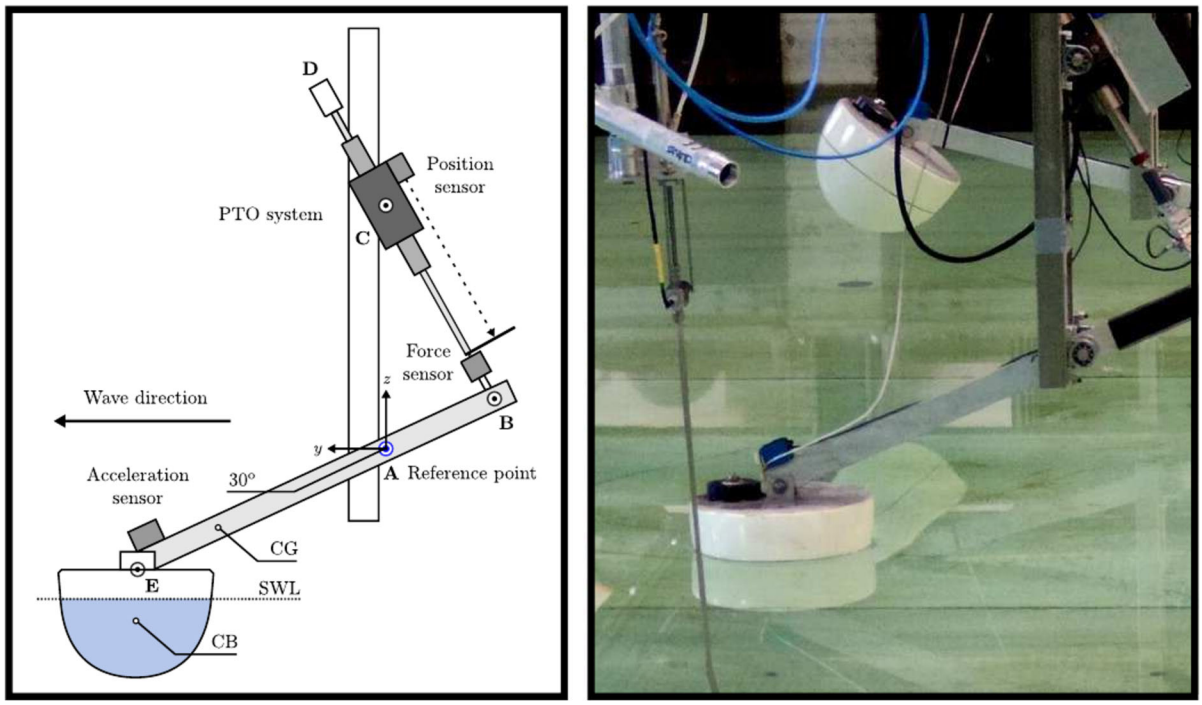


Fig. 4 On the left-hand side: schematic representation of the Wavestar prototype unit used in the experimental campaign. Adapted from [40]. On the right-hand side: photo of the prototype.

consists of a floater mechanically hinged to a fixed reference point above the water surface (point **A** in Fig. 4). At equilibrium, the floater arm is positioned at approximately 30° with respect to the still water level (SWL). It is important to note that the WEC is allowed to move in a single DoF. The main parameters of the baseline prototype are summarised in Table 1. The power take-off (PTO) system employed is an electrical direct-drive linear motor (*LinMot Series P01-37 x 240F*), mounted on the upper structural joint of the device, as depicted in Fig. 4.

The control system is implemented on a Speedgoat Real-time Target Machine, equipped with all necessary modules to handle input/output (I/O) variables. The system is connected via standard Ethernet to the host PC, with data transfer using the User Datagram Protocol. Data acquisition is performed at a consistent sampling rate of 200 [Hz] for all variables throughout the experimental campaign.

Table 1 Main parameters of the WEC system

Parameter	Value	Unit
Floater mass	4	[kg]
Mass moment of inertia w.r.t. **A**	1	[kg m^2]
Floater draft	0.110	[m]
Floater diameter at SWL	0.256	[m]
Equilibrium position w.r.t. **A**	0.523	[rad]
Distance **A**–**C** $L_{\mathbf{AC}}$	0.412	[m]
Distance **C**–**B** $L_{\mathbf{CB}}$ (in eq.)	0.381	[m]
Distance **A**–**B** $L_{\mathbf{AB}}$	0.200	[m]
Distance **A**–**E** $L_{\mathbf{AE}}$	0.484	[m]
Distance **A**–**E** in y	0.437	[m]
Distance **A**–**E** in z	0.210	[m]
Centre of gravity in y	0.415	[m]
Centre of gravity in z	−0.206	[m]
Centre of buoyancy in y	0.437	[m]
Centre of buoyancy in z	−0.321	[m]
Arm mass	1.157	[kg]
Arm moment of inertia w.r.t. **A**	0.060	[kg m^2]

Adapted from [40]

3.2 Test schedule

While a white- or grey- box modelling approach is typically preferred for dynamic analysis, experimen-

tal investigations can leverage black-box modelling to synthesise effective control actions and evaluate WEC performance, particularly when significant uncertainties on the system structure are present. Moreover, given the inherent nonlinear nature of the real systems, the best linear representation [41,42] of the system can be effectively adopted for model-based control.

Therefore, in this experimental investigation, tests have been designed to identify the best linear approximation of the real system, in a black-box fashion, as described in [42]. According to the schematic representation in Fig. 1b), two distinct series of tests are conducted:

- *Identification tests*: These tests employ banded spectra (e.g., banded white noise spectra as proposed in [40]) to characterise the overall system dynamics in an I/O black box modelling framework. The goal is to identify the complete system response, and the tests can be categorised as follows:
  - *Force measurement*: By restraining the Wavestar while it is excited by waves, and measuring the resulting forces, it is possible to characterise the system response described by G_1.
  - *Excitation*: In the absence of wave excitation, the system dynamics described by the map G_2 can be determined by actuating the controlled DoF (through the PTOs) and measuring the associated force-to-velocity relationship.[3]
- *Validation tests*: These tests use real-world (scaled) sea state (SS) conditions to validate the identified model and evaluate the performance of the controlled device under realistic operating conditions.

It is important to note that, while the Wavestar can be easily restrained (locked) for force measurement tests, in practice, this may not always be straightforward. Consequently, an alternative approach to obtaining the G_1 map is through *free motion* tests. This involves exciting the system in uncontrolled conditions to capture the wave-to-velocity map (*i.e.,* $G_\star$ as described in Sect. 2.3).

The wave excitation conditions tested during this experimental campaign are summarised in Table 2. For irregular wave conditions, the period and height refer to the peak period and significant wave height, respectively. The statistical distribution of the wave is represented herein by the JONSWAP spectrum [43], which is a characteristic spectrum for enclosed seas. This spectrum can be defined, according to the parameters in Table 2, as a function of the peak period (or frequency), significant wave height (proportional to the square root of the area), and the parameter $\gamma \in [1, \ldots, 7]$, representing the peak enhancement factor.

A graphical description of the parameters on the wave spectrum is provided in Fig. 5. Please note that all the spectra are drawn with the same significant wave height (i.e., the same area and consequently, the same energy content), and the same peak frequency. The parameter γ modifies the shape of the spectrum and the associated frequency distribution. A common value for enclosed seas is 3.3, while for the third wave (SS3), a peak factor of 1 is chosen to excite a broader range of frequencies.

3.3 Results

The system response is depicted in Fig. 6. Please note that, the system velocity is indicated with $\dot{\theta}$, which defines the angular velocity w.r.t. point **A** (see Fig. 4). Given the nonlinear nature of the system, it is essential to select a range of excitation conditions to fully characterise the system response across different excitation amplitudes. In this study, three different excitation signals are employed, as indicated by the thick grey lines, while the averaged response maps are represented by the bold black lines.[4] We would like to emphasise the importance of selecting representative excitation conditions in terms of both amplitude and frequency. Since the control actions are synthesised by leveraging the IM principle, which is based on linear assumptions, the representativeness of the associated linear model is fundamental.

As discussed in Sect. 2.1, effective control synthesis via IM requires selecting the appropriate matching

[3] Please note that, a detailed analysis of such tests is not provided within this study, being already well-known and defined in the current literature [14,21,35]. For further details, the interesting reader can refer to [40], in which the G_2 map is identified for the Wavestar device.

[4] Although a partial understanding of the system dynamics is necessary to define a sufficiently large frequency bandwidth, the amplitude can be determined by matching the energy content of the excitation conditions to that of the real sea state conditions, as discussed in [40].

Table 2 Wave conditions tested during this experimental investigation

ID	Type	Period [s]	Height [m]	γ	Duration [s]
Identification tests					
WN1	White noise	[0.5, 10]	0.01	–	300
WN2	White noise	[0.5, 10]	0.03	–	300
WN3	White noise	[0.5, 10]	0.05	–	300
Validation tests					
SS1	JONSWAP	1.412	0.063	3.3	300
SS2	JONSWAP	1.836	0.104	3.3	300
SS3	JONSWAP	0.988	0.0208	1	300

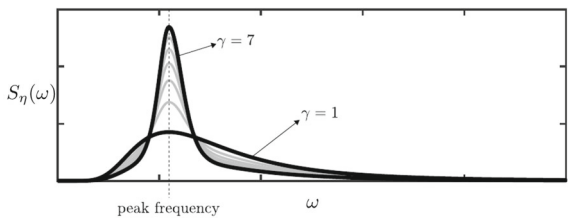
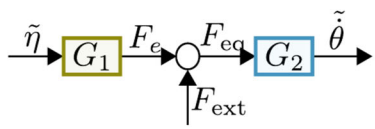


Fig. 5 Representation of the JONSWAP wave spectrum

frequency. In contrast to devices where the controlled DoFs differ from the hydrodynamic ones (see [36] for further details), in the case of the Wavestar, the differences between the wave spectrum and the excitation force spectrum are minimal due to the non-resonant nature of the map G_1. The slight differences between the wave and force spectra can be observed, for example, in Fig. 7 for SS2.

Therefore, the matching frequency is chosen as the peak frequency of each wave spectrum. By achieving the IM-based controller as the complex conjugate of the system impedance, control parameters can be defined based on a specified controller structure. We would like to remark how this method is widely adopted in wave energy field [9,16,22], and it represents a fundamental step to avoid the non-causality of the complex-conjugate operator. In this campaign, a proportional-integral (PI) controller is used to optimise power output and evaluate system performance. Please note that,



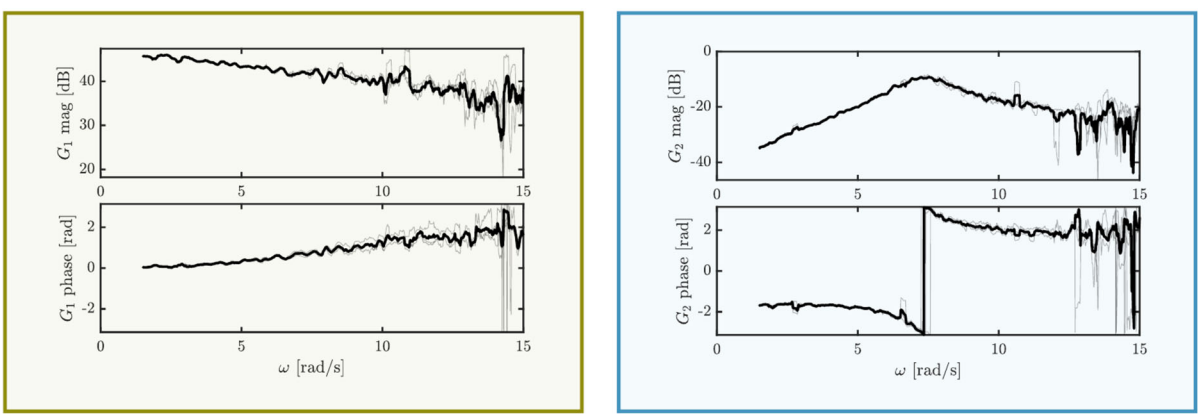


Fig. 6 Best linear approximation of the system wave-to-force and force-to-velocity map. The black bold line refer to the averaged values w.r.t. the thick grey ones

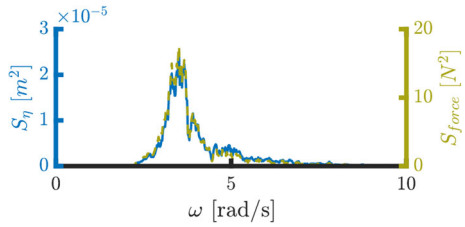


Fig. 7 Wave and force spectrum for the SS2

while the PI structure is adopted herein to achieve control synthesis, the developed methodology serves a broader range of controllers, as a consequent extension of the IM application for WECs. The controller parameters are defined as:

$$\begin{aligned} k_i &= -\omega_m \Im(H_G^{\text{opt}}(\omega_m)), \quad k_p = \Re(H_G^{\text{opt}}(\omega_m)), \\ k_{i,c} &= -\omega_m \Im(H_{G,c}^{\text{opt}}(\omega_m)), \quad k_{p,c} = \Re(H_{G,c}^{\text{opt}}(\omega_m)), \end{aligned} \tag{15}$$

where $\{k_i, k_{i,c}\} \in \mathbb{R}$ are the integral controller parameters for the unconstrained and constrained IM-based condition cases, respectively, and $\{k_p, k_{p,c}\} \in \mathbb{R}$ are the corresponding proportional parameters. In Fig. 8, the interpolation achieved with the experimentally optimized structure is shown to clarify the interpolation procedure and the definition of the implementable controller. It can be observed that the PI control structure effectively matches the optimal control structure at the matching frequency, while the interpolated controller can significantly deviate from the optimal one over a broader frequency range. This issue arises when the exciting force spans a wide frequency range. However, it should be noted that the wave input is generally a narrow-band signal, and the wave-to-force map typically behaves as a band-pass filter [36]. For the sake of clarity, it can also be observed that in the analysed case, the map G_1 shown in Fig. 6 closely behaves as a zero-phase filter, exerting minimal influence on the wave excitation spectrum, as further highlighted in Fig. 7.

Closed-loop stability is not inherently guaranteed by the choice of controller parametrisation (i.e. the controller is not inherently passive). Therefore, the system closed-loop stability has been assessed from a practical perspective by checking the resulting linear model I/O stability.

Table 3 presents the control parameters. It is important to note that, for a reactive PI controller as used here, the addition of a *real* impedance only affects the proportional parameter. This is because the reactive integral part aims to "tune" the system resonance to the excitation frequency. Therefore, the constrained action is achieved by increasing the proportional damping. The parameters arising from the proposed constrained IM-based procedure are selected to halve the system velocity standard deviation in unconstrained IM conditions. To achieve this, the added impedance is computed as the solution of an optimisation problem, i.e. by minimising the value of the added impedance I_a, subject to the constraint described in Ω.

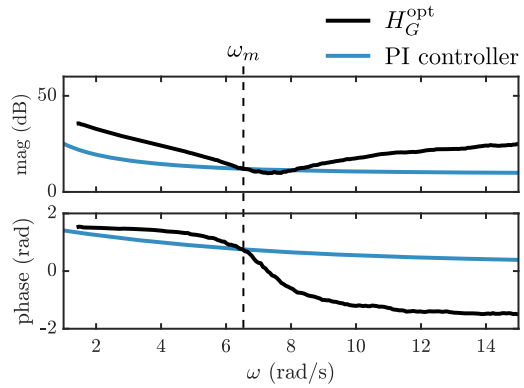


Fig. 8 Example of the interpolation of the PI control structure with the optimal one for the SS3

Table 3 Control parameters for each sea state

Sea State	k_i	k_p	$k_{i,c}$	$k_{p,c}$
SS1	−52.06	2.82	−52.06	9.26
SS2	−67.36	2.58	−67.36	8.48
SS3	−17.77	2.90	−17.77	9.75

We wish to emphasise that the constrained approach proposed and applied herein focuses on limiting the system velocity. Constraining the prototype response is crucial for achieving reliable performance during an experimental campaign. This is because the control action, synthesised using a model-based controller, relies on linear assumptions. If the controller pushes the system beyond these linear assumptions, such as driving the Wavestar on the verge of the waterline, the synthesised control actions and the associated power performance may not accurately represent the system's behaviour.

Figure 9 presents the velocity results for the WEC. Taking advantage of the force measurement tests described in Sect. 3.2, it is possible to appreciate a detailed, zoomed comparison among the system velocity in constrained and unconstrained conditions, and

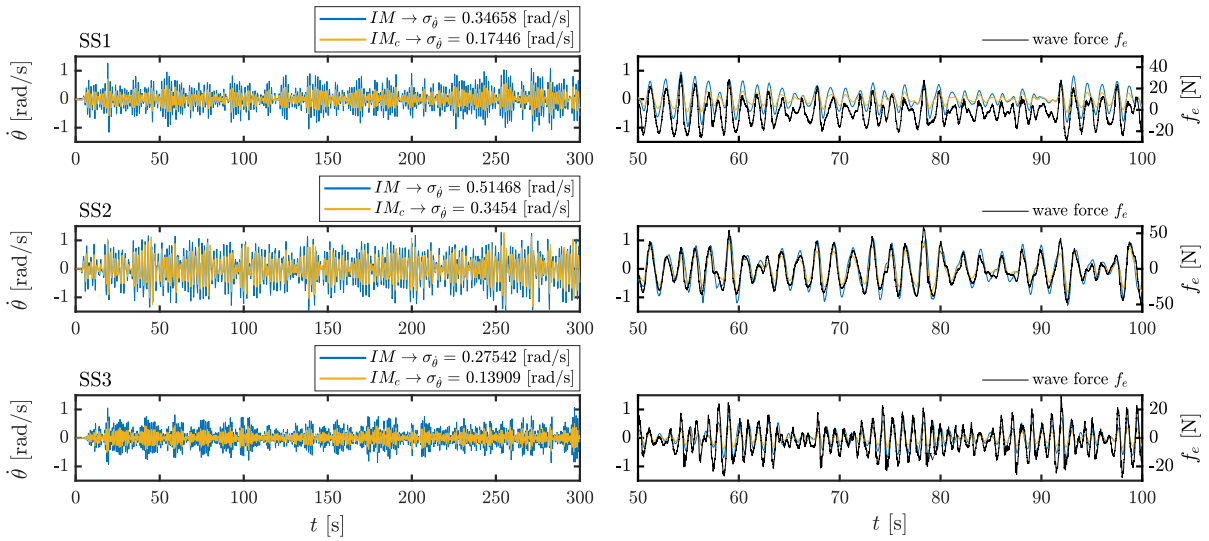


Fig. 9 The floater velocity $\dot{\theta}$ under constrained and unconstrained conditions (blue and yellow, respectively). The plot includes a zoomed-in view on the right-hand side. Furthermore, on the right-hand side the wave excitation force is reported (in black).

the wave exciting force. It is evident that the proposed constrained IM procedure, designed to satisfy the phase synchronisation specified by the impedance principle, respect such condition. Consequently, the velocities in both constrained and unconstrained cases are phase-aligned.

Additionally, by analysing the control parameters and wave data reported in Table 3 and 2, we observe that while SS2 represents the most energetic exciting sea state, it is also the most distant from the system resonance. Specifically, the system resonance is approximately at 7.5 [rad/s] (refer to Fig. 6), which results in a higher integral component of the controller for SS2, i.e., a higher reactive power is needed to tune the system resonance to the exciting wave condition. In contrast, SS3 corresponds to the resonant wave condition, and it is possible to appreciate that the instantaneous power is produced almost entirely by active power, i.e., in the case of a PI controller, generated by the proportional term of the controller. It is closer to the system resonance in terms of peak period and features a peak enhancement factor of 1, which produces a broad banded spectrum. This flatter spectrum distributes wave components across a broader range of frequencies, thus exciting the system resonance more effectively. The resulting constrained system response ratio is:

$$\frac{\sigma_{\dot{\theta},c}}{\sigma_{\dot{\theta}}} = [0.503, 0.671, 0.505], \tag{16}$$

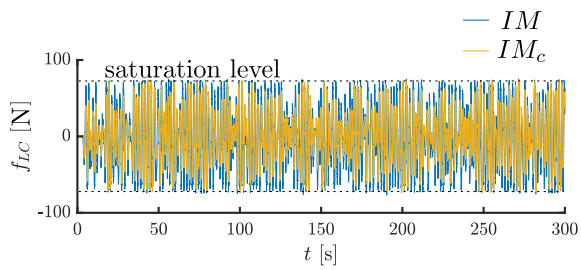


Fig. 10 Control force measured by the load cell (f_{LC}, as shown in Fig. 4) for SS2 under constrained and unconstrained conditions

for SS1, SS2, and SS3, respectively. While for SS1 and SS3 the constrained controller effectively halves the system response, its performance is less effective for SS2.

This performance discrepancy can be attributed to the force limitations imposed by the hardware. Although the IM strategy aims to maximise energy harvesting, which can require potentially large forces, the actual applied force is constrained by a driver saturation limit of 60 [N] to prevent damage. Consequently, the controller cannot fully adhere to the IM conditions, leading to suboptimal performance for the constrained controller. This issue is exacerbated by the fact that SS2, while being the most energetic sea state tested, is also the furthest from the system resonance condition. In Fig. 10, the controller force measured at the load cell is

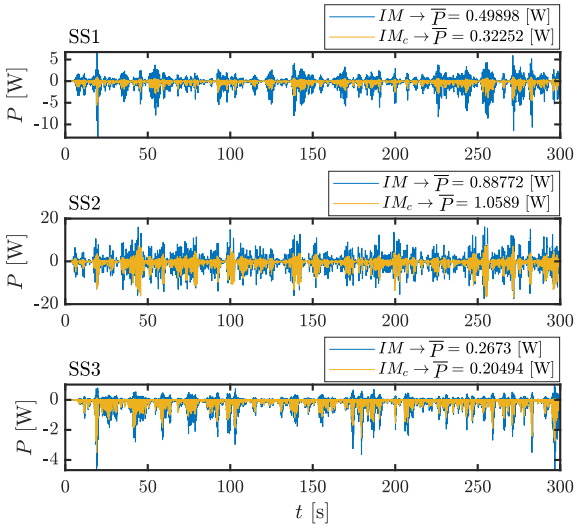


Fig. 11 Instantaneous power output for all tested conditions. The mean absorbed power is indicated by $\overline{P}$

shown for SS2, illustrating how PTO saturation significantly limits the control action in unconstrained conditions. While the constraint handling approach proposed and implemented within this study aims to reduce the system velocity, a side effect is a significant reduction in overall control actions. Although the constrained condition results in less effective control and a reduction in harvested energy for SS2, the presence of saturations in a real scenario leads to a loss of representativeness of the adopted model, thereby introducing errors in the definition of control actions. This outcome can be observed by analysing the power output presented in Fig. 11.

For SS1 and SS3, the constrained controller, by adhering to the imposed constraints, approaches a suboptimal control synthesis, which results in reduced power absorption.We would like to remark that, in the case of the aforementioned sea states, given the absence of saturation effects and the accurately identified model, the control synthesis is highly effective. By leveraging the IM principle in unconstrained conditions, it is possible to provide a representative control action that effectively maximises the power output of the system. Furthermore, in constrained conditions, the target constraint (of limiting the motion to 50%) is perfectly met, as shown in Eq. (16).

However, when hard constraints are present, this outcome is not necessarily true. In fact, the constrained controller can achieve higher power harvesting compared to the unconstrained one, as it operates more effectively within the saturation limits.

Synthesising a controller with an impedance-based approach offers a significant advantage in simplicity. However, when the system exhibits significant nonlinearities, the importance of synthesising a control action capable of constraining the device response becomes crucial. The results demonstrate that the proposed constrained approach effectively confines the device within the desired parameters, highlighting the importance of a constraint-handling strategy when nonlinearities are present, as these can lead to a loss of representativeness in the model.

4 Conclusions

The IM principle represents a powerful tool for defining a straightforward yet effective control strategy for wave energy systems. However, this technique is inherently based on linear assumptions, meaning the control action may no longer be effective when operating conditions push the model outside its range of validity. While the applications of IM extend across various domains, experimental investigations remain a crucial step in the development of marine energy technologies, such as WECs. In this context, evaluating system performance can be particularly challenging when control actions are synthesised using model-based approaches, as uncertainties related to prototyping can be significant.

This paper proposes a constrained methodology for impedance-based control within a generalised modelling framework, demonstrating how the control action can constrain the device motion while still respecting the impedance phase condition. The proposed control strategy is experimentally tested and compared against unconstrained conditions using the Wavestar prototype at the Aalborg experimental facility. The identified model accurately represents the system, allowing the controller to confine device motion within predefined limits. Furthermore, the performance of the constrained controller is evaluated under nonlinear force saturation conditions, demonstrating a significant increase in power output, as the synthesised constrained control action more accurately reflects real-world operational conditions.

Acknowledgements The authors would like to express their sincere gratitude to Mr. H.S. Kassen for the inestimable support during the experimental campaign.

Author contributions B.P. wrote the main manuscript of the paper and developed the methodology. B.P., M. G., L.D., R.D., N.F., F.F., executed the experimental campaign. F.F. and G.M. supervised the work. All the authors reviewed the manuscript.

Funding Open access funding provided by Politecnico di Torino within the CRUI-CARE Agreement. Project founded from the Ministry of University and Research and PNRR's PhD scholarship program defined in DM-118/2023. This publication is part of the project PNRR-NGEU. Project funded under the National Recovery and Resilience Plan (NRRP), Italy, Mission 4 Component 2 Investment 1.3 - Call for tender No. 1561 of 11.10.2022 of Ministero dell' Universitá e della Ricerca (MUR); funded by the European Union - NextGenerationEU Award Number: Project code PE0000021, Concession Decree No. 1561 of 11.10.2022 adopted by Ministero dell'Universitá e della Ricerca (MUR), Italy, CUP, Italy E13C22001890001, Project title "Network 4 Energy Sustainable Transition - NEST". Nicolás Faedo acknowledges the project funded by the European Union - NextGenerationEU under the National Recovery and Resilience Plan (NRRP), Mission 04 Component 2 Investment 3.1 | Project Code: IR0000027 - CUP: B33C22000710006 - iENTRANCE@ENL: Infrastructure for Energy TRAnsition aNd Circular Economy @ EuroNanoLab.

Data availability No datasets were generated or analysed during the current study.

Declarations

Competing interests The authors declare no competing interests.

Open Access This article is licensed under a Creative Commons Attribution 4.0 International License, which permits use, sharing, adaptation, distribution and reproduction in any medium or format, as long as you give appropriate credit to the original author(s) and the source, provide a link to the Creative Commons licence, and indicate if changes were made. The images or other third party material in this article are included in the article's Creative Commons licence, unless indicated otherwise in a credit line to the material. If material is not included in the article's Creative Commons licence and your intended use is not permitted by statutory regulation or exceeds the permitted use, you will need to obtain permission directly from the copyright holder. To view a copy of this licence, visit http://creativecommons.org/licenses/by/4.0/.

References

1. IEA, IRENA, UNSD, WorldBank, and WHO. Tracking SDG 7: The energy progress report (2023)
2. Foteinis, S.: Wave energy converters in low energy seas: current state and opportunities. Renew. Sustain. Energy Rev. **162**, 112448 (2022). https://doi.org/10.1016/j.rser.2022.112448
3. Faedo, N., Peña-Sanchez, Y., Ringwood, J.V.: Finite-order hydrodynamic model determination for wave energy applications using moment-matching. Ocean Eng. **163**, 251–263 (2018)
4. Ringwood, J.V., Zhan, S., Faedo, N.: Empowering wave energy with control technology: possibilities and pitfalls. Ann. Rev. Control **55**, 18–44 (2023). https://doi.org/10.1016/j.arcontrol.2023.04.004
5. Ringwood, J.V.: Wave energy control: status and perspectives 2020. In: IFAC World Congress (2020)
6. Pasta, E., Faedo, N., Mattiazzo, G., Ringwood, J.V.: Towards data-driven and data-based control of wave energy systems: classification, overview, and critical assessment. Renew. Sustain. Energy Rev. **188**, 113877 (2023). https://doi.org/10.1016/j.rser.2023.113877
7. Ringwood, J.V., Merigaud, A., Faedo, N., Fusco, F.: Wave energy control systems: Robustness issues. In: Proceedinds of the IFAC Conference on control Aplications in Marine Systems, Robotics, and Vehicles, (2018). https://doi.org/10.1016/j.ifacol.2018.09.470
8. Floyd, T.L., Pownell, E.: Principles of electric circuits. PEARSON INDIA (2000)
9. Faedo, N., Carapellese, F., Pasta, E., Mattiazzo, G.: On the principle of impedance-matching for underactuated wave energy harvesting systems. Appl. Ocean Res. **118**, 102958 (2022). https://doi.org/10.1016/J.APOR.2021.102958
10. Scruggs, J.T.: On the causal power generation limit for a vibratory energy harvester in broadband stochastic response. J. Intell. Mater. Syst. Struct. **21**, 1249–1262 (2010). https://doi.org/10.1177/1045389X10361794. (**Cited by: 48**)
11. Ringwood, J.V., Mérigaud, A., Faedo, N., Fusco, F.: An analytical and numerical sensitivity and robustness analysis of wave energy control systems. IEEE Trans. Control Syst. Technol. **28**, 1337–1348 (2020). https://doi.org/10.1109/TCST.2019.2909719
12. Ringwood, J.V., Tom, N., Ferri, F., Yu, Y.-H., Coe, R.G., Ruehl, K., Bacelli, G., Shi, S., Patton, R.J., Tona, P., Sabiron, G., Merigaud, A., Ling, B.A., Faedo, N.: The wave energy converter control competition (WECCCOMP): Wave energy control algorithms compared in both simulation and tank testing. Appl. Ocean Res. **138**, 103653 (2023). https://doi.org/10.1016/j.apor.2023.103653
13. Ringwood, J., Ferri, F., Tom, N., Ruehl, K., Faedo, N., Bacelli, G., Yu, Y.-H., Coe, R.: The wave energy converter control competition: Overview. In: International Conference on Offshore Mechanics and Arctic Engineering, vol. 6 (2019). https://doi.org/10.1115/OMAE2019-95216
14. Faedo, N., Pasta, E., Carapellese, F., Orlando, V., Pizzirusso, D., Basile, D., Sirigu, S.A.: Energy-maximising experimental control synthesis via impedance-matching for a multi degree-of-freedom wave energy converter. IFAC-PapersOnLine **55**, 345–350 (2022). https://doi.org/10.1016/j.ifacol.2022.10.453. 14th IFAC Conference on Control Applications in Marine Systems, Robotics, and Vehicles CAMS 2022
15. Robertson, A., Bachynski, E.E., Gueydon, S., Wendt, F., Schünemann, P.: Total experimental uncertainty in hydrodynamic testing of a semisubmersible wind turbine, considering numerical propagation of systematic uncertainty.

Ocean Eng. **195**, 106605 (2020). https://doi.org/10.1016/J.OCEANENG.2019.106605
16. Coe, R.G., Bacelli, G., Forbush, D.: A practical approach to wave energy modeling and control. Renew. Sustain. Energy Rev. **142**, 110791 (2021). https://doi.org/10.1016/j.rser.2021.110791
17. Paduano, B., Pasta, E., Carapellese, F., Papini, G., Baltazar, J., Faedo, N., Mattiazzo, G.: Control co-design mooring optimisation for wave energy systems: a three-tethered point absorber case. IFAC-PapersOnLine **56**, 11717–11722 (2023). https://doi.org/10.1016/j.ifacol.2023.10.537. 22nd IFAC World Congress
18. Coe, R.G., Bacelli, G., Olson, S., Neary, V.S., Topper, M.B.R.: Initial conceptual demonstration of control co-design for WEC optimization. Journal of Ocean Engineering and Marine Energy **6**, 441–449 (2020). https://doi.org/10.1007/s40722-020-00181-9
19. Penalba, M., Giorgi, G., Ringwood, J.V.: Mathematical modelling of wave energy converters: a review of nonlinear approaches. Renew. Sustain. Energy Rev. **78**, 1188–1207 (2017). https://doi.org/10.1016/j.rser.2016.11.137
20. Windt, C., Faedo, N., Penalba, M., Dias, F., Ringwood, J.V.: Reactive control of wave energy devices—the modelling paradox. Appl. Ocean Res. **109**, 102574 (2021). https://doi.org/10.1016/j.apor.2021.102574
21. Vervaet, T., Quartier, N., Moreno, E.C., Fernandez, G.V., Ferri, F., Stratigaki, V., Troch, P.: System identification and centralised causal impedance matching control of a row of two heaving point absorber wave energy converters. Ocean Eng. **309**, 118399 (2024). https://doi.org/10.1016/j.oceaneng.2024.118399
22. García-Violini, D., Peña-Sanchez, Y., Faedo, N., Ringwood, J.V.: An energy-maximising linear time invariant controller (lite-con) for wave energy devices. IEEE Transactions on Sustainable Energy **11**, 2713–2721 (2020). https://doi.org/10.1109/TSTE.2020.2971392
23. García-Violini, D., Peña-Sanchez, Y., Faedo, N., Windt, C., Ringwood, J.V.: LTI energy-maximising control for the wave star wave energy converter: identification, design, and implementation??this material is based upon work supported by science foundation ireland under grant no. 13/ia/1886. IFAC-PapersOnLine **53**, 12313–12318 (2020). https://doi.org/10.1016/j.ifacol.2020.12.1193. 21st IFAC World Congress
24. Galeani, S., Tarbouriech, S., Turner, M., Zaccarian, L.: A tutorial on modern anti-windup design. Eur. J. Control. **15**, 418–440 (2009). https://doi.org/10.3166/ejc.15.418-440
25. Faedo, N., Carapellese, F., Papini, G., Pasta, E., Mosquera, F.D., Ferri, F., Brekken, T.K.A.: An anti-windup mechanism for state constrained linear control of wave energy conversion systems: Design, synthesis, and experimental assessment. IEEE Trans. Sustain. Energy **15**, 964–973 (2024). https://doi.org/10.1109/TSTE.2023.3320190
26. ITTC. Ittc recommended guidelines, wave energy converter model test experiments (2011)
27. Zhou, X., Zhang, H., Jin, H., Liu, C., Xu, D.: Numerical and experimental investigation of a hinged wave energy converter with negative stiffness mechanism. Int. J. Mech. Sci. **245**, 108103 (2023). https://doi.org/10.1016/j.ijmecsci.2023.108103
28. Windt, C., Davidson, J., Ransley, E.J., Greaves, D., Jakobsen, M., Kramer, M., Ringwood, J.V.: Validation of a CFD-based numerical wave tank model for the power production assessment of the wavestar ocean wave energy converter. Renew. Energy **146**, 2499–2516 (2020). https://doi.org/10.1016/j.renene.2019.08.059
29. Babarit, A., Delhommeau, G.: Theoretical and numerical aspects of the open source BEM solver NEMOH. In: Proceedings of the 11th European Wave and Tidal Energy Conference, pp. 1–12, (2015)
30. Faltinsen, O.: Sea Loads on Ships and Offshore Structures. Cambridge University Press, Cambridge (1993)
31. Folley, M.: Numerical Modelling of Wave Energy Converters—State of the Art Techniques for Single Devices and Arrays. Elsevier, Amsterdam (2016)
32. Carapellese, F., Pasta, E., Paduano, B., Faedo, N., Mattiazzo, G.: Intuitive LTI energy-maximising control for multi-degree of freedom wave energy converters: the PeWEC case. Ocean Eng. (2022). https://doi.org/10.1016/j.oceaneng.2022.111444
33. Faedo, N., Peña-Sanchez, Y., Carapellese, F., Mattiazzo, G., Ringwood, J.V.: LMI-based passivation of LTI systems with application to marine structures. IET Renew. Power Gener. **15**, 3424–3433 (2021). https://doi.org/10.1049/rpg2.12286
34. Carapellese, F., Pasta, E., Sirigu, S.A., Faedo, N.: SWINGO: conceptualisation, modelling, and control of a swinging omnidirectional wave energy converter. Mech. Syst. Signal Process. **197**, 110356 (2023). https://doi.org/10.1016/j.ymssp.2023.110356
35. Paduano, B., Edoardo, P., Faedo, N., Mattiazzo, G.: Control synthesis via impedance-matching in panchromatic conditions: a generalised framework for moored systems. In: European Wave and Tidal Energy Conference, pp. 344 (2023). https://doi.org/10.36688/ewtec-2023-344
36. Paduano, B., Faedo, N., Mattiazzo, G.: On the effect of wave direction on control and performance of a moored pitching wave energy conversion system. J. Mar. Sci. Eng. **11**, 2001 (2023). https://doi.org/10.3390/jmse11102001
37. Liu, K., Chen, D., Liang, P., Yao, X., Deng, Z., Xu, K., Xin, Y., Huang, D.: SPH modeling and experimental validation on power performance and dynamic response of a novel swing-wing wave energy converter. Energy Convers. Manag. **325**, 119420 (2025). https://doi.org/10.1016/j.enconman.2024.119420
38. Huang, S., Tang, X., Wang, K., Zhou, F.: Fully coupled time-domain dynamic analyses and actual sea state experimental validation of a multi-body floating wave energy converter. Energy **321**, 135133 (2025). https://doi.org/10.1016/j.energy.2025.135133
39. Hansen, R.H., Kramer, M.M.: Modelling and control of the wavestar prototype. In: Proceedings of the 9th European Wave and Tidal Energy Conference (2011)
40. Faedo, N., Peña-Sanchez, Y., Pasta, E., Papini, G., Mosquera, F.D., Ferri, F.: Swell: an open-access experimental dataset for arrays of wave energy conversion systems. Renew. Energy **212**, 699–716 (2023). https://doi.org/10.1016/j.renene.2023.05.069
41. Schoukens, J., Ljung, L.: Nonlinear system identification: a user-oriented road map. IEEE Control Syst. Mag. **39**, 28–99 (2019). https://doi.org/10.1109/MCS.2019.2938121

42. Pintelon, R., Schoukens, J.: System Identification: A Frequency Domain Approach, 2nd edn. Wiley, Hoboken (2012)
43. World Meteorological Organization. Guide to Wave Analysis and Forecasting. Secretariat of the World Meteorological Organization, 1988. ISBN 9789263107022

Publisher's Note Springer Nature remains neutral with regard to jurisdictional claims in published maps and institutional affiliations.